Journal of Materials and Construction
ISSN 2734-9438
Website: www. jomc.vn

Nonlinear inelastic behaviors of concrete-filled steel tubular beam-column structures

Ho Ngoc Khoa[1], Le Thi Phuong Loan[1], Luu Van Thuc[1], Vu Chi Cong[1*]

[1] Faculty of Building and Industrial Construction, Hanoi University of Civil Engineering

KEYWORDS

Advanced analysis CFST
Stability function Beam-column element
Distributed plasticity model

ABSTRACT

A new advanced method combining stability function and distributed plasticity model has been developed using Fortran programming language to predict the nonlinear inelastic behavior of concrete-filled steel tubalar (CFST) under static loading. The advantage of this method is the ability to accurately study the nonlinear behavior using only one or two beam-column elements per member instead of using solid and shell elements as traditional methods, thereby improving the model analysis time. The Generalized Displacement Control (GDC) algorithm, capable of analyzing beyond the limit point, will be used to solve the nonlinear equilibrium equations instead of the traditional Newton-Raphson algorithm. The element stiffness matrix is integrated through the Gauss-Lobatto numerical integration framework, while the nonlinear geometric effects P-Δ and P-δ are considered using stability functions and a corresponding geometric matrix. The reliability and accuracy of the proposed method are verified by comparing the analysis results with experimental data. The obtained results have demonstrated that using beam-column elements for simulation, the proposed method still provides accurate results while significantly reducing computational resources. Therefore, this new method holds promise as a useful tool for practical design and analysis of statically loaded CFST structures.

1. Introduction

In recent years, concrete-filled steel tube (CFST) structures have become increasingly popular in the construction of buildings and bridges due to their high strength, durability, good ductility, and ability to absorb large amounts of energy [1-4]. CFST structures typically consist of steel tubes filled with high-strength or medium-strength concrete, with typical cross-sections as shown in Figure 1, and are often used for compression. The compressive strength of the concrete core is significantly increased by the confinement effect from the outer steel tubes, as shown in Figure 2. Meanwhile, the steel tube structure is restrained by its inner concrete, leading to an increase in the local buckling resistance of the steel tubes compared to conventional steel tubes [1], as illustrated in Figure 3. Furthermore, the elimination of formwork in the concrete construction process reduces costs and construction time [1], as shown in Figure 4. Therefore, to be able to understand and apply this type of structure, many experimental studies have been conducted recently [5-9]. Although observing the behavior of CFST structures through experiments can be reliable, this method is expensive, time-consuming, and not suitable for all situations. Therefore, using numerical simulation tools would be an effective alternative for studying the behavior of these structures.

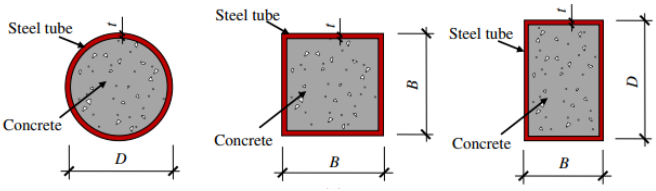

Figure 1. The typical structure of a CFST.

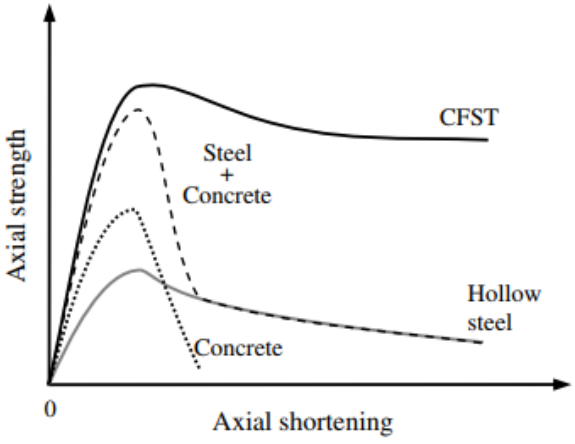

Figure 2. Comparion of the relationship between load-deformation of steel tube columns, concrete columns, and corresponding CFST columns.

*Corresponding author: congvc@huce.edu.vn
Received 15/04/2024, Revised 15/05/2024, Accepted 23/05/2024
Link DOI: https://doi.org/10.54772/jomc.v14i01.717

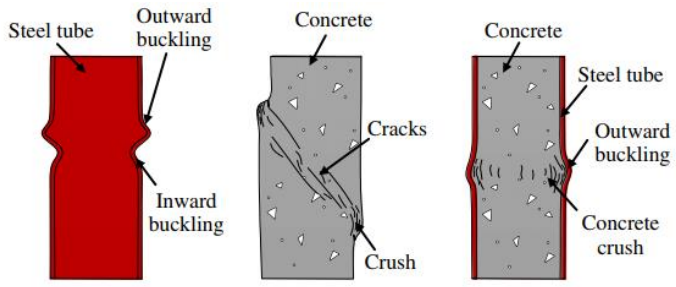

Figure 3. The failure mode of steel tube columns, concrete columns, and corresponding CFST columns.

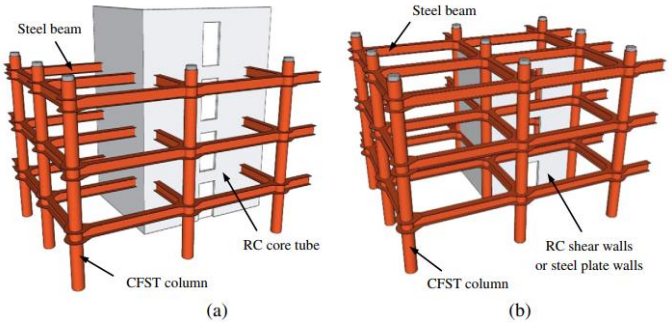

Figure 4. Hybrid structural systems using CFST columns in high-rise buildings.

Until now, numerical methods used to study the behavior of CFST structures often rely on commercial software package such as Abaqus, Ls-dyna, and Ansys [10-13]. It can be observed that the elements used in commercial software package to simulate CFST structures are usually block elements and shell elements. This makes the simulation process time-consuming, complex in many situations, and imposes limitations on the practical design process [14,15]. To overcome this limitation, a fiber beam-column model (fiber model) will be developed for CFST structural analysis in this study. In this fiber model, the cross-sections at integration points will be divided into multiple small fibers, and the stress-strain relationship will be clearly observed throughout the analysis process, allowing for the observation of deformation distribution on the cross-section and along the element. Note that advanced analysis methods need to consider both nonlinear sources, including geometric and material nonlinearity. For geometric nonlinearity, it can be considered using displacement interpolation functions as in traditional finite element methods or using stability functions [16]. Because displacement interpolation functions are formed based on the displacement field, they cannot accurately predict geometric nonlinear behavior P-δ when only one or two elements are used on a member. Therefore, to obtain accurate solutions, this method requires the use of multiple elements on a member, leading to a decrease in computational efficiency. This limitation can be overcome by using stability functions. This is because stability functions allow for an accurate consideration of the geometric nonlinear effect P-δ with only one or two elements. To the best of the author's knowledge, this method has been developed for nonlinear analysis of steel structures and has been shown to be significantly more efficient than commercial software packages [16-18]. However, there seems to be no study on the nonlinear analysis of CFST structures using stability functions. Therefore, stability functions will be developed in this study.

In this study, a novel advanced method combining stability functions and distributed plasticity model will be developed using Fortran programming language to predict the nonlinear behavior of CFST structures under static loading. The advantage of this method is the ability to accurately study nonlinear behavior with only one or two beam-column elements per member instead of using traditional block and shell elements, thereby improving the model analysis time. The GDC algorithm with post-peak analysis capability will be used to solve nonlinear equilibrium equations instead of the traditional Newton-Raphson algorithm. The element stiffness matrix will be integrated through the Gauss-Lobatto quadrature framework while geometric nonlinear effects P-δ and P-Δ will be considered using stability functions and corresponding geometric matrices. The reliability and accuracy of the proposed method will be validated through comparison of analysis results with experimental data. The results have demonstrated that, with the use of beam-column elements for simulation, the proposed method still provides accurate results while significantly reducing computational resources. Therefore, this new method promises to be a useful tool for practical design and analysis of CFST structures under static loading.

2. The formulas for the proposed CFST beam-column element

2.1. Basic Assumptions

Below are the assumptions in the process of constructing the fiber beam-column element

(1) The cross-section remains flat and perpendicular to the axis of the element after deformation.

(2) The bond between steel and concrete is considered perfect.

(3) Large displacements and rotations are permitted, but deformations are small.

(4) Torsional effects are not considered.

2.2. Geometric nonlinearity source due to second-order effects P-δ

To study the nonlinear geometric effects due to the interaction between axial force and bending moment of the beam-column element P-δ, this study utilized the stability function developed by Chen et al. [19]. The main advantage of the stability function is its ability to consider geometric nonlinear behavior P-δ with only one or two elements on a beam-column member, thereby significantly reducing the analysis time of the model. By considering a beam-column element with two-way bending curvature as shown in Figure 5, the relationship between force and displacement of that element can be derived, as formulated by Kim et al. [20], as follows :

$$\Delta F = K_e \Delta d \quad (1)$$

$$\Delta F = [\Delta P \quad \Delta M_{yi} \quad \Delta M_{yj} \quad \Delta M_{zi} \quad \Delta M_{zj} \quad \Delta T]^T \quad (2)$$

$$\Delta d = [\Delta \delta \quad \Delta \theta_{yi} \quad \Delta \theta_{yj} \quad \Delta \theta_{zi} \quad \Delta \theta_{zj} \quad \Delta \phi]^T \quad (3)$$

$$K_e = \begin{bmatrix} \frac{EA}{L} & 0 & 0 & 0 & 0 & 0 \\ 0 & S_{iy}\frac{EI}{L} & S_{jy}\frac{EI}{L} & 0 & 0 & 0 \\ 0 & S_{jy}\frac{EI}{L} & S_{iy}\frac{EI}{L} & 0 & 0 & 0 \\ 0 & 0 & 0 & S_{iz}\frac{EI}{L} & S_{jz}\frac{EI}{L} & 0 \\ 0 & 0 & 0 & S_{jz}\frac{EI}{L} & S_{iz}\frac{EI}{L} & 0 \\ 0 & 0 & 0 & 0 & 0 & \frac{GJ}{L} \end{bmatrix} \quad (4)$$

where P is the axial force, M_{yi}, M_{yj}, M_{zi}, and M_{zj} are the moments at the two ends of the element corresponding to the y and z axes; T is the torsional moment; δ is the axial deformation; θ_{yi}, θ_{yj}, θ_{zi}, and θ_{zj} are the rotations of the nodes at the two ends of the element corresponding to the y and z axes; φ is the twist angle; G is the shear modulus; E is the elastic modulus of the material; J is the torsional constant of the cross-section; A is the cross-sectional area; L is the length of the element; S_{1n} and S_{2n} (n = y,z) are the stability functions corresponding to the y and z axes, and they are determined by the following equations:

$$S_{1n} = \begin{cases} \frac{\pi\sqrt{\rho_n}[\sin(\pi\sqrt{\rho_n}) - \pi\sqrt{\rho_n}\cos(\pi\sqrt{\rho_n})]}{2 - 2\cos(\pi\sqrt{\rho_n}) - \pi\sqrt{\rho_n}\sin(\pi\sqrt{\rho_n})} & \text{if} P < 0 \\ \frac{\pi\sqrt{\rho_n}[\pi\sqrt{\rho_n}\cosh(\pi\sqrt{\rho_n}) - \sinh(\pi\sqrt{\rho_n})]}{2 - 2\cosh(\pi\sqrt{\rho_n}) + \pi\sqrt{\rho_n}\sinh(\pi\sqrt{\rho_n})} & \text{if} P > 0 \end{cases} \quad (5)$$

$$S_{2n} = \begin{cases} \frac{\pi\sqrt{\rho_n}[\pi\sqrt{\rho_n} - \sin(\pi\sqrt{\rho_n})]}{2 - 2\cos(\pi\sqrt{\rho_n}) - \pi\sqrt{\rho_n}\sin(\pi\sqrt{\rho_n})} & \text{if} P < 0 \\ \frac{\pi\sqrt{\rho_n}[\sinh(\pi\sqrt{\rho_n}) - \pi\sqrt{\rho_n}]}{2 - 2\cosh(\pi\sqrt{\rho_n}) + \pi\sqrt{\rho_n}\sinh(\pi\sqrt{\rho_n})} & \text{if} P > 0 \end{cases} \quad (6)$$

where $\rho_n = P/(\pi^2 EI_n/L^2)$, where P is positive if the axial force is tension and negative if the axial force is compression.

EA represents the axial stiffness of the fiber beam-column element, while EI_n and GJ represent the flexural stiffness and torsional stiffness of that element, respectively. These values are determined based on the following formulas:

$$EA = \sum_{t=1}^{s} w_t \left(\sum_{i=1}^{m} E_i A_i\right)_t \quad (7)$$

$$EI_y = \sum_{t=1}^{s} w_t \left(\sum_{i=1}^{m} E_i A_i z_i^2\right)_t \quad (8)$$

$$EI_z = \sum_{t=1}^{s} w_t \left(\sum_{i=1}^{m} E_i A_i y_i^2\right)_t \quad (9)$$

$$GJ = \sum_{t=1}^{s} G w_t \left[\sum_{i=1}^{m} (y_i^2 + z_i^2) A_i\right]_t \quad (10)$$

where s is the number of axial distributed integration points of the beam-column element; m is the number of fibers in a cross-section at an integration point; w_k is the corresponding integration weight; E_i is the elastic modulus of the i^{th} material; A_i is the area of the i^{th} fiber; and y_i and z_i are the local coordinates of the i^{th} fiber in the cross-section, corresponding to the *z* and *y* axes, respectively.

2.3. Nonlinear material source

To observe the gradual spread of plastic deformation across a cross-section, this paper will utilize the fiber beam-column element model. The basic principle of the fiber beam-column element is that a single element will be divided into multiple segments through integration points. At each integration point, the cross-section of that element will be further subdivided into a matrix of fibers, each characterized by parameters such as area Ai, local coordinates corresponding to the centroid (y_i, z_i), and residual stress if considered. Then, each fiber will be assigned a different material model, and these models will be updated at each load increment during the analysis process. The deformation of the cross-section is characterized by three components: axial deformation ε and two curvature components χ_z and χ_y corresponding to the local y and z axes. The corresponding internal forces include axial force N and bending moments about the two axes M_z and M_y. Forces and deformations of the cross-section are grouped into rows.

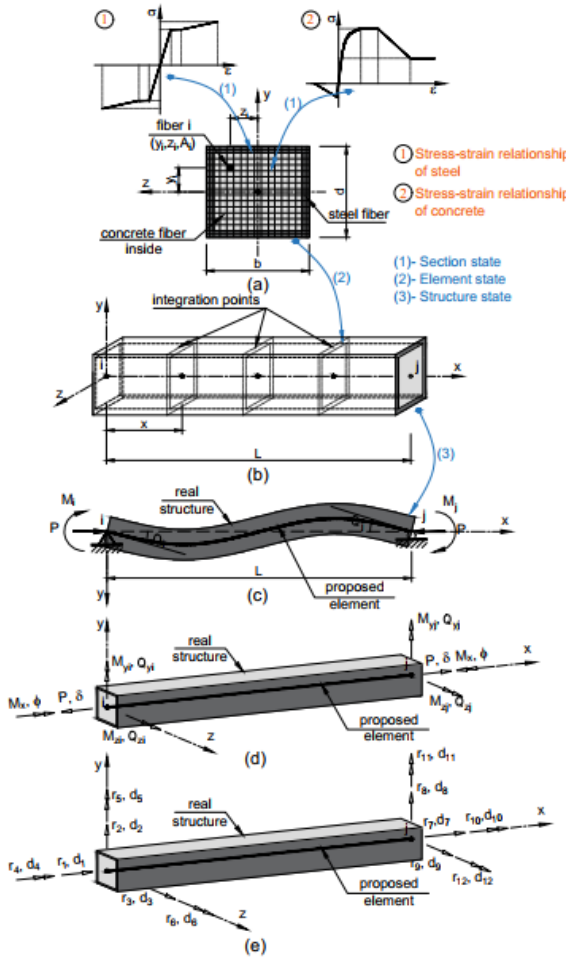

Figure 5. The proposed fiber beam-column element for CFST structural analysis.

The cross-section force vector **Q** and the incremental force vector on the cross-section **ΔQ**

$$Q = [M_z(x) \quad M_y(x) \quad N(x)]^T \quad (11)$$

$$\Delta Q = [\Delta M_z \quad \Delta M_y \quad \Delta N]^T \quad (12)$$

The deformation vector **q** and the incremental deformation vector on the cross-section **Δq**

$$q = [\chi_z(x) \quad \chi_y(x) \quad \varepsilon(x)]^T \quad (13)$$

$$\Delta q = [\Delta\chi_z \quad \Delta\chi_y \quad \Delta\varepsilon]^T \quad (14)$$

The force on the cross-section **Q** at each integration point is calculated based on the element nodal force **F** and the interpolation force matrix as the expression below

$$\Delta Q = B(x)\Delta F \quad (15)$$

$$B(x) = \begin{bmatrix} \delta_y(\zeta L) & 0 & 0 & (\zeta-1) & \zeta & 0 \\ -\delta_z(\zeta L) & (\zeta-1) & \zeta & 0 & 0 & 0 \\ 1 & 0 & 0 & 0 & 0 & 0 \end{bmatrix}; \zeta = \frac{x}{L} \quad (16)$$

where $\delta_y(\zeta L)$ and $\delta_z(\zeta L)$ are the corresponding lateral displacement components along the local z and y axes. These values are determined based on the following expressions

$$\delta_y(\zeta L) = -\frac{1}{EI_z k_z^2}\left\{M_{zi}\left[\frac{\sin(k_z\zeta L)}{\tan(k_z L)} - \cos(k_z\zeta L) - \zeta + 1\right] + M_{zj}\left[\frac{\sin(k_z\zeta L)}{\sin(k_z L)} - \zeta\right]\right\} \quad (17)$$

$$\delta_z(\zeta L) = \frac{1}{EI_y k_y^2}\left\{M_{yi}\left[\frac{\sin(k_y\zeta L)}{\tan(k_y L)} - \cos(k_y\zeta L) - \zeta + 1\right] + M_{yj}\left[\frac{\sin(k_y\zeta L)}{\sin(k_y L)} - \zeta\right]\right\} \quad (18)$$

Then, the deformation of the cross-section will be determined based on the cross-section force as follows

$$\Delta q = k_{sec}^{-1} Q \quad (19)$$

in which the stiffness matrix of the cross-section is calculated according to the following expression:

$$k_{sec}^{-1} \sum_{i=1}^{m} E_i A_i \begin{bmatrix} y_i^2 & (-y_i)z_i & (-y_i) \\ (-y_i)z_i & z_i^2 & z_i \\ (-y_i) & z_i & 1 \end{bmatrix} \quad (20)$$

Based on the assumption that the cross-section will remain flat and perpendicular to the element axis after deformation, the incremental deformation vector of the axial fibers is determined through the incremental deformation of the cross-section as follows:

$$\Delta\varepsilon_i(x,y,z) = a_i^T \Delta q \quad (21)$$

where $\mathbf{a}_i$ is the linear geometric matrix, and this matrix is determined by the following expression:

$$a_i = \{-y_i \quad z_i \quad 1\}^T \quad (22)$$

After the deformation of the fibers has been determined, the incremental stress and tangent modulus of each fiber are also updated based on different stress-strain models. During the iteration process, the element stiffness matrix $\mathbf{K}_e$ and the cross-section stiffness matrix $\mathbf{k}_{sec}$ will be continuously updated after each load increment. Based on the new tangent modulus, the centroid position of the cross-section will also be updated in each load increment to consider the distribution of plasticity of the cross-section. The internal forces of the cross-section are calculated by summing up the axial forces and bending moments of all fibers, as described in the equation below:

$$Q_r = \begin{Bmatrix} M_z(x) \\ M_y(x) \\ N(x) \end{Bmatrix} = \sum_{i=1}^{m} \sigma_i A_i \begin{Bmatrix} -y_i \\ z_i \\ 1 \end{Bmatrix} = \sum_{i=1}^{m} \sigma_i A_i a_i \quad (23)$$

2.4. Nonlinear geometric source due to second-order effects P-δ

The nonlinear geometric effect P-Δ due to the rotation of elements in the frame will be described in this section. Figure 5 (c) illustrates the relationship between force and displacement at the nodes of the beam-column element, while Figure 5 (d) describes the sign convention of the corresponding forces and displacements. The dynamic relationship and equilibrium of the beam-column element can be inferred by comparing these two figures and are expressed as follows

$$\Delta f_n = T^T \Delta F \quad (24)$$

$$\Delta d = T\Delta d_L \quad (25)$$

$$\Delta f_n^T = \{\Delta r_1 \quad \Delta r_2 \quad \Delta r_3 \quad \Delta r_4 \quad \Delta r_5 \quad \Delta r_6 \quad \Delta r_7 \quad \Delta r_8 \quad \Delta r_9 \quad \Delta r_{10} \quad \Delta r_{11} \quad \Delta r_{12}\} \quad (26)$$

$$\Delta d_L^T = \{\Delta d_1 \quad \Delta d_2 \quad \Delta d_3 \quad \Delta d_4 \quad \Delta d_5 \quad \Delta d_6 \quad \Delta d_7 \quad \Delta d_8 \quad \Delta d_9 \quad \Delta d_{10} \quad \Delta d_{11} \quad \Delta d_{12}\} \quad (27)$$

where $\Delta\mathbf{f}_n$ and $\Delta\mathbf{d}_L$ are the nodal force and displacement vectors, respectively, of a finite beam-column element; $\Delta\mathbf{F}$ and $\Delta\mathbf{d}$ are the nodal force and displacement vectors of the beam-column element, while **T** is the transformation matrix and is calculated as follows:

$$T = \begin{bmatrix} -1 & 0 & 0 & 0 & 0 & 0 & 1 & 0 & 0 & 0 & 0 & 0 \\ 0 & 0 & -\frac{1}{L} & 0 & 1 & 0 & 0 & 0 & \frac{1}{L} & 0 & 0 & 0 \\ 0 & 0 & -\frac{1}{L} & 0 & 0 & 0 & 0 & 0 & \frac{1}{L} & 0 & 1 & 0 \\ 0 & \frac{1}{L} & 0 & 0 & 0 & 1 & 0 & -\frac{1}{L} & 0 & 0 & 0 & 0 \\ 0 & \frac{1}{L} & 0 & 0 & 0 & 0 & 0 & -\frac{1}{L} & 0 & 0 & 0 & 1 \\ 0 & 0 & 0 & 1 & 0 & 0 & 0 & 0 & 0 & -1 & 0 & 0 \end{bmatrix} \quad (28)$$

Through the transformation matrix from the dynamic relationship and equilibrium, the relationship between nodal force and displacement vectors is determined as follows:

$$\Delta f_n = K_n \Delta d_L \quad (29)$$

where $\mathbf{K}_n$ is the element stiffness matrix, and this matrix is calculated according to the expression:

$$K_n = T^T K_e T \quad (30)$$

Equation (25) is applied for the case of a beam-column element without the ability to rotate. However, if the element is able to rotate, axial and shear forces will increase within the element. These increased forces can be related to nodal displacements through the following equation:

$$\Delta f_s = K_g \Delta d_L \quad (31)$$

where $\mathbf{K}_g$ is the element stiffness matrix due to the rotational effects of the frame components, and this matrix is determined as follows:

$$K_g = \begin{bmatrix} K_s & -K_s \\ -K_s^T & K_s \end{bmatrix} \quad (32)$$

where

$$\mathbf{K}_s = \begin{bmatrix} 0 & \left(M_{zi}+M_{zj}\right)/L^2 & \left(M_{yi}+M_{yj}\right)/L^2 & 0 & 0 & 0 \\ \left(M_{zi}+M_{zj}\right)/L^2 & P/L & 0 & 0 & 0 & 0 \\ \left(M_{yi}+M_{yj}\right)/L^2 & 0 & P/L & 0 & 0 & 0 \\ 0 & 0 & 0 & 0 & 0 & 0 \\ 0 & 0 & 0 & 0 & 0 & 0 \\ 0 & 0 & 0 & 0 & 0 & 0 \end{bmatrix} \quad (33)$$

By comparing equations (24) and (29) with each other, the relationship between the force and displacement of the beam-column element can be calculated according to the following formula:

$$\Delta f_L = K\,\Delta d_L \quad (34)$$

here

$$\Delta f_L = \Delta f_n + \Delta f_s \quad (35)$$

$$K = K_n + K_g \quad (36)$$

3. Constitutive model

3.1. Stress-strain relationship for structural steel

Structural steel sections can be produced through hot rolling or cold forming processes. The relationship between stress and strain of the steel sections in this paper is described by a three-stage model, as

suggested by Tai et al. [21]. This material model is illustrated in Figure 6 and equation (37). The initial stage of deformation is assumed to be fully elastic. Then, upon reaching the yield limit, the steel's deformation increases while stress remains constant, and finally, the material enters the hardening stage. Similar to the behavior of steel bars, the tensile and compressive behaviors of structural steel sections are also assumed to be equivalent

$$f_s = \begin{cases} E_s\varepsilon_s \; if 0 \le |\varepsilon_s| \le \varepsilon_y \\ \pm f_y \; if \varepsilon_y < |\varepsilon_s| \le \varepsilon_h \\ \pm\left[f_y + E_h(|\varepsilon_s| - \varepsilon_h)\right] if \varepsilon_h < |\varepsilon_s| \le \varepsilon_u \end{cases} \quad (37)$$

where the parameter E_s represents the elastic modulus of the steel section, f_s and ε_s are the corresponding stress and strain in the steel section, f_y and ε_y denote the yield stress and yield strain, and f_u is the ultimate stress. It should be noted that strain hardening is chosen as $\varepsilon_s = 0{,}005$ for high-strength steel and $\varepsilon_h = 10\varepsilon_y$ for structural steel, and the ultimate strain is $\varepsilon_u = 0{,}1$ for high-strength steel and $\varepsilon_u = 0{,}2$ for structural steel.

3.2. *Stress-strain relationship of confined concrete*

The box-shaped steel structure serves to confine the lateral expansion of the concrete core, thereby leading to a significant improvement in both the strength and ductility of concrete in CFST structures. In this study, the stress-strain relationship of confined concrete will be modeled as shown in Figure 7, based on the research by Mander et al. [22]. The initial stage of tension extends from 0 to a strain value ε within the compression zone and is represented as follows

$$\sigma_c = \frac{f_{cc}^{'} kr}{r-1+k^r} \quad (38)$$

here

$$k = \frac{\varepsilon_c}{\varepsilon_{cc}^{'}} \quad (39)$$

where σ_c is the compressive strength while ε_c is the corresponding compressive strain.

$$r = \frac{E_c}{E_c - \left(\frac{f_{cc}^{'}}{\varepsilon_{cc}^{'}}\right)} \quad (40)$$

Detailed information about the parameters E_c, f'_{cc}, ε'_{cc}, the strength reduction factor, and the confinement pressure causing lateral confinement of concrete can be found in the studies by Liang [23]. Accordingly, the confined compressive strength of concrete in the steel tube is determined as follows

$$\sigma_c = \begin{cases} f_{cc}^{'} \;\; if \varepsilon_{cc}^{'} \le \varepsilon_c \le \varepsilon_{cu1} = 0{,}005 \\ 100(f_{cc}^{'} - \alpha_c f_{cc}^{'})(0{,}015 - \varepsilon_c) + \alpha_c f_{cc}^{'} \;\; if \varepsilon_{cu1} = 0{,}005 < \varepsilon_c \le \varepsilon_{cu2} = 0{,}015 \\ \alpha_c f_{cc}^{'} \;\; if \varepsilon_c > \varepsilon_{cu2} = 0{,}015 \end{cases} \quad (41)$$

For the concrete region under tension, the tensile stress is assumed to increase linearly up to a value $0{,}6\sqrt{f_{cc}^{'}}$ with a corresponding tensile strain increasing until concrete cracks. After concrete cracking, the tensile stress is assumed to decrease linearly to a value of 0.

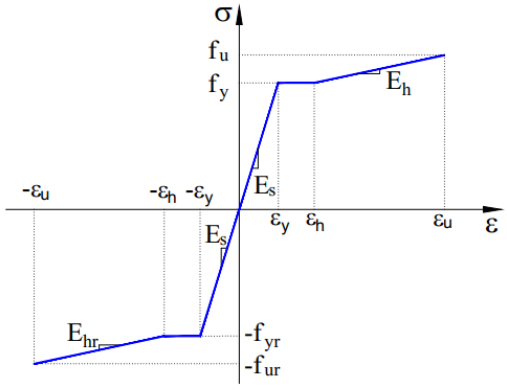

Figure 6. The stress-strain relationship of the structural steel used in the study.

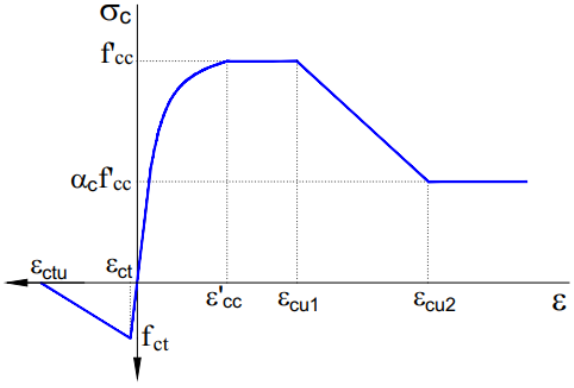

Figure 7. The stress-strain relationship of the confined concrete used in the study.

4. Nonlinear incremental-iterative solution procedure

The fundamental issue of the nonlinear analysis problem involves solving a series of nonlinear equilibrium equations of the structure. During the process of variable loading, the stiffness of the structure may change, leading to fluctuations in the equilibrium path, which can be stable or not. The Newton-Raphson method is an iterative method that helps solve nonlinear problems quickly. Although this method can be applied to most types of structures to find the relationship between load and displacement, it is only suitable within the load-bearing capacity of the structure. When the load exceeds the structure's load-bearing limit, the convergence process will fail. To observe the equilibrium process of the structure when exceeding the allowed load limit, an analysis with decreased load steps must be conducted, which cannot be achieved by the traditional Newton-Raphson method. Therefore, the GDC method developed by Yang and colleagues [24] will be used to address nonlinear problems with multiple load limit points and snap-back points. This method has been widely used recently due to its effectiveness and numerical stability. Hence, the GDC method is applied in this paper to analyze the nonlinear behaviors of the structure, as illustrated in Figure 8.

The GDC method has three main features: (1) the ability to

automatically adjust the loading step; (2) the capability to change the loading direction when the load reaches a critical point; and (3) numerical stability in the restricted region. In the j-th iteration of the i-th load increment, the incremental form of the equilibrium equation can be represented as follows :

$$K_{j-1}^{i}\Delta D_{j}^{i} = \lambda_{j}^{i}\hat{P} + R_{j-1}^{i} \quad (42)$$

$$\hat{P} = K_{j-1}^{i}\Delta\hat{D}_{j}^{i} \quad (43)$$

$$R_{j-1}^{i} = K_{j-1}^{i}\Delta\bar{D}_{j}^{i} \quad (44)$$

Replacing equation (43) and equation (44) into equation (42)

$$\Delta D_{j}^{i} = \lambda_{j}^{i}\Delta\hat{D}_{j}^{i} + \Delta\bar{D}_{j}^{i} \quad (45)$$

where ΔD_{j}^{i} is the incremental displacement vector, $\Delta\hat{D}_{j}^{i}$ is the incremental displacement vector generated by the reference load vector $\hat{P}$, $\Delta\bar{D}_{j}^{i}$ is the incremental displacement vector generated by the unbalanced force vector R_{j-1}^{i}, K_{j-1}^{i} is the stiffness matrix, and λ_{j}^{i} is the load increment parameter.

The total displacement vector D_{j}^{i}, the applied load vector $\hat{P}$, and the load factorΛ_{j}^{i} of the structure at the end of the j-th iteration of the i-th load increment are accumulated as follows:

$$\Lambda_{j}^{i} = \Lambda_{j-1}^{i} + \lambda_{j}^{i} \quad (46)$$

$$P_{j}^{i} = \Lambda_{j}^{i}\hat{P} \quad (47)$$

$$D_{j}^{i} = D_{j-1}^{i} + \Delta D_{j}^{i} \quad (48)$$

In the first iteration (j=1), the load increment parameter λ_{j}^{i} is calculated as follows

$$\lambda_{1}^{i} = \lambda_{1}^{1}\sqrt{|GSP|} \quad (49)$$

where GSP is the generalized stiffness parameter and λ_{1}^{1} represents the initial value of the load increment parameter, which is calculated as follows:

$$GSP = \frac{\Delta\hat{D}_{1}^{1^{T}}\Delta\hat{D}_{1}^{1}}{\Delta\hat{D}_{1}^{i-1^{T}}\Delta\hat{D}_{1}^{i}} \quad (50)$$

For the next iteration ($j \geq 2$), the value of the load increment parameter λ_{j}^{i} is determined as follows:

$$\lambda_{j}^{i} = -\frac{\Delta\hat{D}_{1}^{i-1^{T}}\Delta\bar{D}_{j}^{i}}{\Delta\hat{D}_{1}^{i-1^{T}}\Delta\hat{D}_{j}^{i}} \quad (51)$$

5. Verification

In this section, two numerical examples will be analyzed to verify the accuracy and computational efficiency of the proposed method in predicting the nonlinear elastic-plastic behavior of CFST structures under static loading. The results obtained from the proposed method will be compared with experimental results. By using the established formulas for beam-column elements, a computer program will be developed in the Fortran programming language for the analysis process.

5.1. CFST column subjected to concentric loading

This example is conducted to verify the accuracy of the proposed method by comparing the results from the proposed method with the results from experiments conducted by some authors. The configuration, dimensions, and cross-section of the CFST column under compressive loading are illustrated in Figure 9 (a) and (b). The model and discretized cross-sections in the proposed program are depicted in Figure 9 (c). The detailed dimensions of the column structure and material properties used are presented in Table 1. To perform the nonlinear analysis, the column structure is modeled by four fiber beam-column elements, with each element using 5 integration points. The axial force-deformation curves and ultimate axial force between the analysis by the proposed program and the experimental results will be used for comparison purposes. Four CFST columns subjected to compression tested by Tomii et al. [8], labeled as C-1, C-2, C-3, and C-4, will be analyzed and verified. The ratio of steel tube thickness to column width, D/t, for these columns ranges from 23,5 to 45,5. The material for these columns is lightweight steel tubes, cold-formed and undergone annealing process to remove residual stresses.

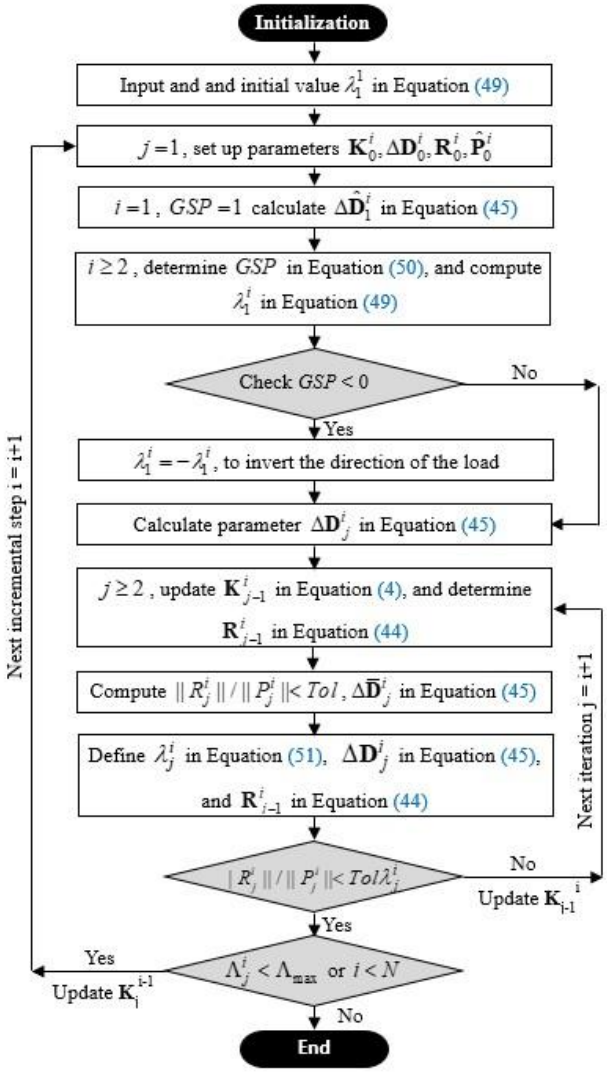

Figure 8. Nonlinear elastic-plastic analysis scheme applied to the GDC algorithm.

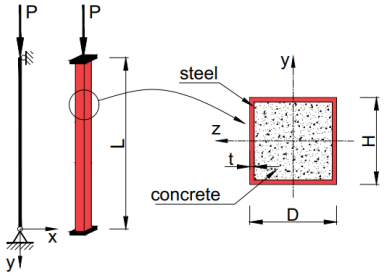

(a) Configuration and corresponding cross-section of the CFST column

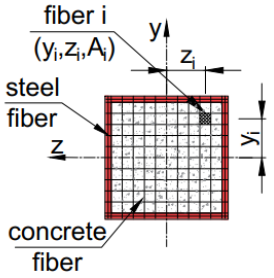

(b) The discretization of the cross-section into fibers in the proposed program

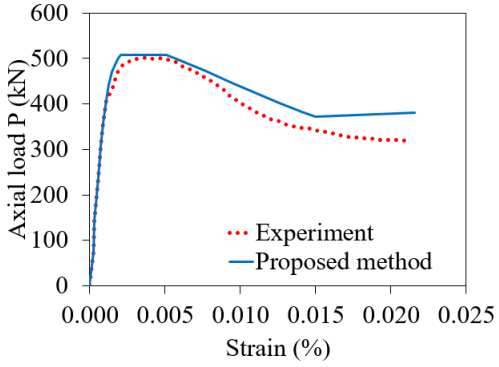

(c) Comparion of the results of specimen C-1

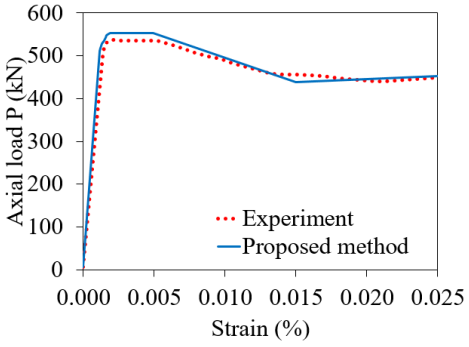

(d) Comparion of the results of specimen C-2

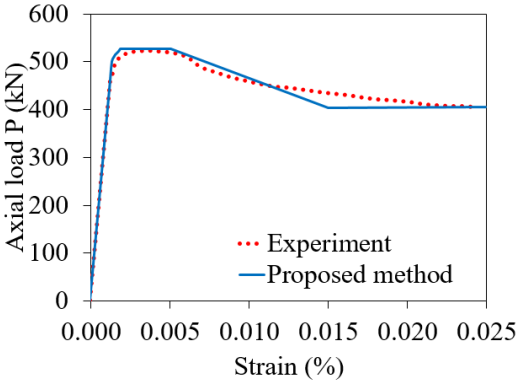

(e) Comparion of the results of specimen C-3

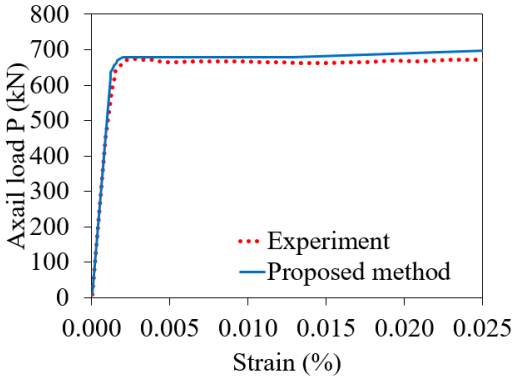

(f) Comparion of the results of specimen C-4

Figure 9. CFST column subjected to concentric loading.

The relationship between axial force-deformation obtained from the proposed method and from experiments is compared in Figures 9 (c) - (f). The analysis results from the proposed program closely resemble the experimental results, with the average value of the ultimate axial force ratio between simulation and experiment $P_{u,pt}/P_{u,tn}$ being 1,02. Therefore, it can be concluded that the proposed method can accurately and effectively consider the nonlinear elastic-plastic behavior of CFST columns under compressive loading.

Table 1. The ultimate axial load of the CFST column under concentric loading.

Column	D (mm)	t (mm)	D/t	f_y (MPa)	f'_c (MPa)	$P_{u.tn}$ (kN)	$P_{u.pt}$ (kN)	$\frac{P_{u.pt}}{P_{u.tn}}$	Ref.
C-1	100	2,29	43,7	197	38,4	507	509,3	1,00	[8]
C-2	100	2,20	45,5	345	25,7	521	527,2	1,01	
C-3	100	2,99	33,4	293	24,7	538	552,1	1,03	
C-4	100	4,25	23,5	289	23,8	680	706,9	1,04	
Average								1,02	
Standard deviation								0,01	

5.2. CFST beam subjected to axial loading and bending

In most cases, beam structures typically only experience the effects of bending and shear. However, in some instances, beams may also have to withstand additional influences from axial forces due to neighboring structures such as bracing frames. In such cases, it is necessary to study the flexural-compressive behavior of beams. The configuration and cross-section of the CFST beam under flexural-compressive loading are simultaneously illustrated in Figure 10 (a). This beam structure has been experimented on by Tomii et al. [8], and will be utilized to verify the accuracy of the proposed program. The model and discretization of the cross-section in the proposed program are presented in Figure 10 (b). The detailed dimensions and material properties of four experimental beam specimens, labeled as D-1, D-2, D-3, and D-4, are compiled in Table 2, where the ratio between the height and the thickness of the steel box, D/t, ranges from 23,5 to 45,5. The load is applied to the beam structure through two stages. In the first stage, an axial force N is applied and it is continuously maintained in the subsequent stage. Then, a bending moment is applied gradually by incrementing the vertical force P. Therefore, the actual moment at the mid-span of the beam is the sum of the moment due to the vertical load P and an additional moment caused by the axial force N and the sway. The influence of local instability phenomena will be examined for the steel tubes in all specimens except for specimen D-4.

The moment-curvature curves analyzed by the proposed program and from experiments are compared in Figures 10 (b) - (e). Despite the significant increase in axial force N, the flexural capacity of the CFST beam does not decrease significantly. The results from the proposed program closely match the experimental results. The ratio of ultimate flexural strength between simulation and experiment $M_{u,pt}$ / $M_{u,tn}$ is 1,02, with a standard deviation of 0,03, as summarized in Table 2. This demonstrates that the proposed method can accurately analyze the nonlinear behavior of CFST beams under flexural-compressive loading.

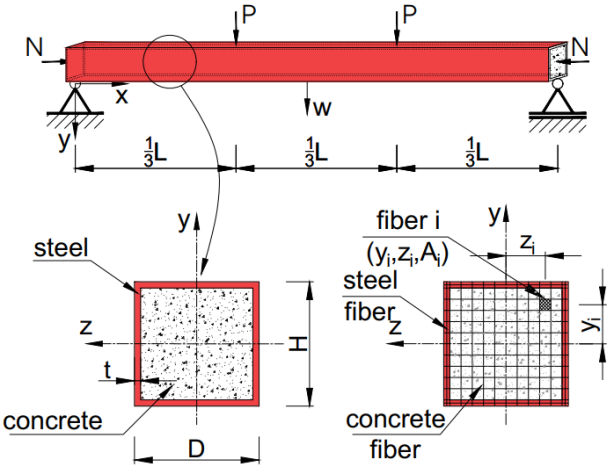

(a) Configuration, cross-section of the beam, and the discretization of the cross-section into fibers in the proposed program

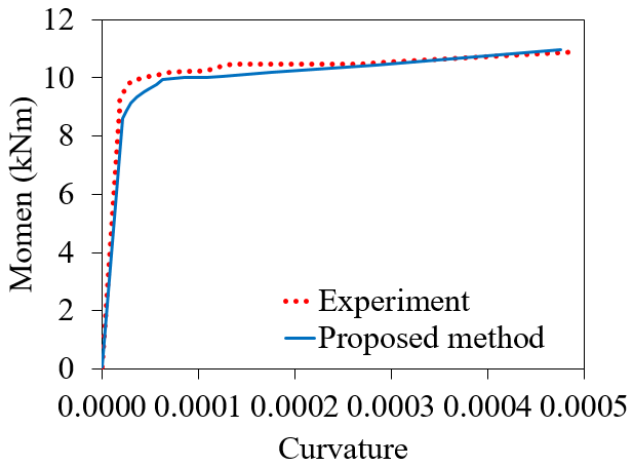

(b) Comparion of the results of specimen D-1

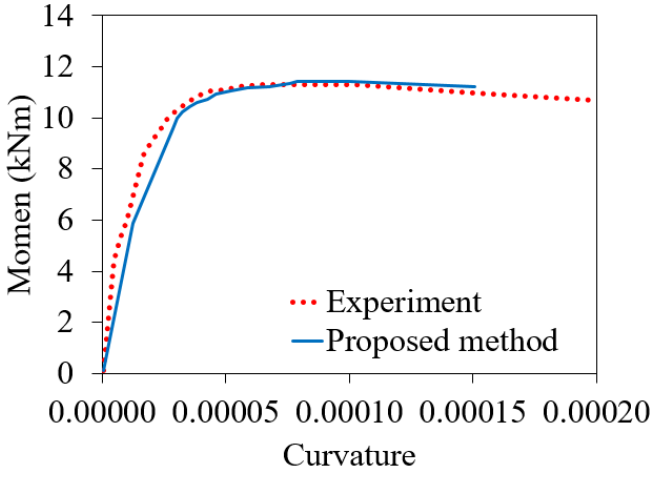

(c) Comparion of the results of specimen D-2

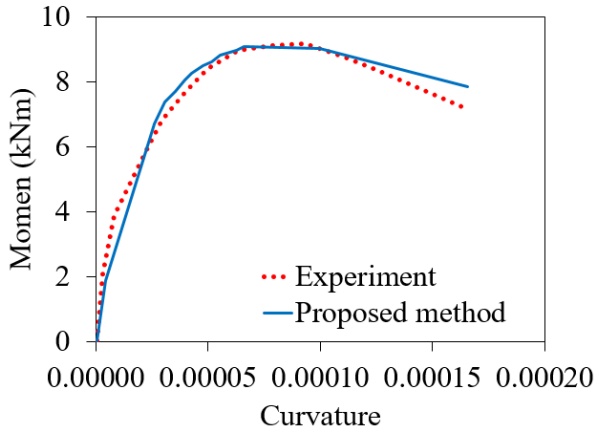

(d) Comparion of the results of specimen D-3

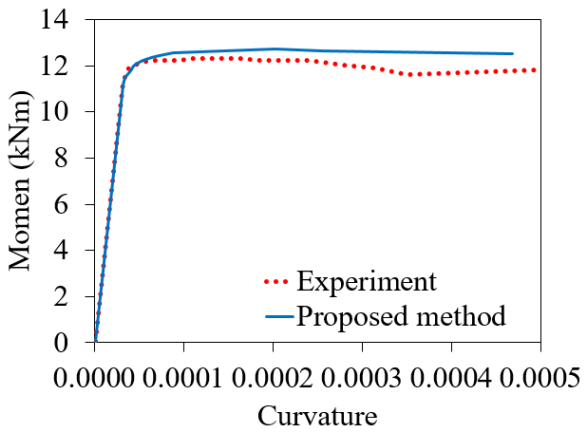

(e) Comparion of the results of specimen D-4

Figure 10. CFST beam under axial loading and bending.

Table 2. The ultimate flexural strength of the CFST beam under flexural-compressive loading.

Beam	D (mm)	t (mm)	D/t	f_y (MPa)	f'_c (MPa)	N (kN)	$M_{u.tn}$ (kN.m)	$M_{u.pt}$ (kN.m)	$\frac{M_{u.pt}}{M_{u.tn}}$	Ref.
D-1	100	2,29	43,7	197	28,8	77,7	10,4	10,4	1,00	[8]
D-2	100	2,29	43,7	197	45,9	194,3	11,4	11,3	0,99	
D-3	100	2,29	43,7	197	44,0	335,8	8,4	9,0	1,07	
D-4	100	2,27	44,1	310	25,9	46,8	12,6	12,7	1,01	
Average									1,02	
Standard deviation									0,03	

6. Case studies

In this section, a composite frame structure using CFST columns subjected to axial and lateral loads in a cyclic form will be studied to verify the practical applicability of the proposed method in structural analysis practice. The composite frame structure, with rigid connections subjected to compressive and cyclic lateral loads, was experimented on by Han et al. [25] and will be utilized to verify the accuracy and analytical capability of the proposed method. The configuration of the SF-22 frame in Han's experimental series [25] and the discretization of the cross-section are illustrated in Figure 11 (a). The column structure is fabricated from square hollow steel sections filled with concrete with a width of 140 mm and a steel thickness of 4 mm. I-shaped steel, with dimensions as shown in Figure 11 (a), is used for the horizontal beams. For the steel box structure, the yield strength and ultimate strength of the steel material are f_{ys} = 361,0 N/mm^2 and f_{us} = 433,8 N/mm^2, and the modulus of elasticity E = 2,062x10^5 MPa. Meanwhile, the yield strength and ultimate strength of the I-shaped steel are f_{ys} = 361,6 N/mm^2 and f_{us} = 495,5 N/mm^2, and the modulus of elasticity E = 2,042x10^5 MPa. The compressive strength of the cubic concrete sample is $f_c^{'}$ = 56,2 MPa and will be converted to cylindrical compressive strength. The load will be applied to the frame through two stages. In the first stage, a compressive force N = 375,0 kN will be applied to the frame at the two upper ends of the column, and this load will be maintained throughout the subsequent lateral loading P process. In the next stage, the lateral load P will be applied at the top of the column and gradually increased.

The curves between lateral load P and corresponding lateral displacement u obtained from analysis by the proposed method and experiment are compared in Figure 11 (b). From Figure 11 (b), it can be observed that the analysis results closely match the experiment in both the early stage, peak stage, and subsequent nonlinear stage. The ultimate lateral load from the proposed method is $P_{u,pt}$ = 148,2 kN, while the corresponding value from the experiment is $P_{u,tn}$ = 154,1 kN, with a difference of less than 3,9%. Therefore, it can be concluded that the proposed program is capable of reliably and accurately analyzing the nonlinear behavior of CFST frame structures using fiber beam-column elements.

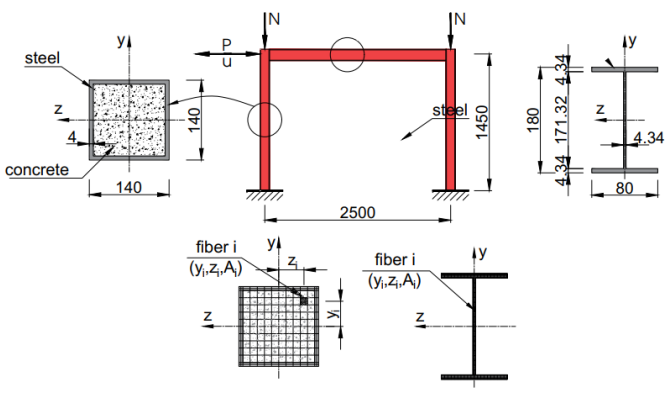

(a) The configuration of the composite frame, corresponding cross-section, and discretization of the cross-section into fibers in the proposed program

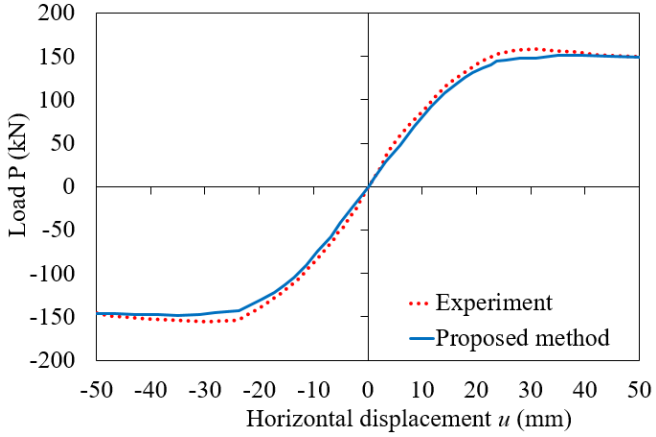

(b) Comparion of the results of the proposed program with experimental results

Figure 11. Composite portal frame subjected to lateral loads.

7. Conclusions

A new advanced method integrating stability functions and distributed plasticity models into fiber beam-column elements has been successfully developed using Fortran programming language to predict the nonlinear elastic-plastic behavior of CFST structures under static loading. The main results obtained are as follows

(1) The proposed method demonstrates the capability to accurately and efficiently analyze the nonlinear inelastic behavior of CFST structures under static loading using beam-column elements. The analysis results obtained from the proposed program closely resemble experimental results for both CFST column structures under compression, CFST beam structures under flexural-compressive loading, and large-sized composite CFST frames. Therefore, the newly proposed method holds promise to provide a new useful tool for practical design and analysis of CFST structures.

(2) Solely utilizing beam-column elements, the proposed method still provides analysis results similar to experiments. This demonstrates the effectiveness of the proposed program in terms of computational resource efficiency compared to other commercial software, as these typically utilize solid and shell elements.

References

[1]. Han Lin-Hai, Li Wei, Bjorhovde Reidar (2014), "Developments and advanced applications of concrete-filled steel tubular (CFST) structures: Members", *Journal of constructional steel research*, 100: 211-228.

[2]. Hoàn Phạm Thái (2021), "Ước lượng khả năng chịu nén đúng tâm của cột ống thép nhồi bê tông bằng thuật toán máy học", *Tạp chí Khoa học Công nghệ Xây dựng (KHCNXD)-ĐHXDHN*, 15 (3V): 69-78.

[3]. Thao Dinh Thi Nhu, Binh Luu Thanh, Phuong Tran Duy, Van Hiep Nguyen, Chinh Truong Hoai, Cuong Ngo Huu (2018), "Phân tích bậc hai phi đàn hồi cột ống thép nhồi bê tông", *Tạp chí Khoa học Công nghệ Xây dựng (KHCNXD)-ĐHXDHN*, 12 (2): 18-23.

[4]. Zarringol Mohammadreza, Thai Huu-Tai, Thai Son, Patel Vipulkumar (2020), "Application of ANN to the design of CFST columns", *Structures*, Elsevier, 2203-2220.

[5]. Huang Fuyun, Yu Xinmeng, Chen Baochun (2012), "The structural performance of axially loaded CFST columns under various loading conditions", *Steel & Composite Structures*, 13 (5): 451-471.

[6]. Kawaguchi Jun, Morino Shosuke, Sugimoto Toshikazu, Shirai Junya, "Experimental study on structural characteristics of portal frames consisting of square CFT columns", in Composite construction in steel and concrete IV, 2002, 725-733.

[7]. Lu Deren, et al. (2021), "Experimental study of square CFST stub columns with a low steel ratio under axial loading", *Frontiers in Materials*, 8: 629819.

[8]. Tomii Masahide, Sakino Kenji (1979), "Experimental studies on the ultimate moment of concrete filled square steel tubular beam-columns", *Transactions of the Architectural Institute of Japan*, 275: 55-65.

[9]. Xiamuxi Alifujiang, Hasegawa Akira (2011), "Compression test of RCFT columns with thin-walledsteel tube and high strength concrete", *Steel and Composite Structures, An International Journal*, 11 (5): 391-402.

[10]. Kopuri NAGK Manikanta, Priyadharshani S Anitha (2022), "Numerical analysis of concrete filled steel tube columns using ABAQUS", *Materials Today: Proceedings*, 65: 3476-3482.

[11]. Lavanya J, Elangovan R (2017), "The structural behaviour of concrete filled steel tubular columns", *International Research Journal of Engineering and Technology*, 4 (6): 209-15.

[12]. Qu Haiyan, Li Guoqiang, Chen Suwen, Sun Jianyun, Sozen Mete A (2011), "Analysis of circular concrete-filled steel tube specimen under lateral impact", *Advances in Structural Engineering*, 14 (5): 941-951.

[13]. Zhou Kan, Han Lin-Hai (2019), "Modelling the behaviour of concrete-encased concrete-filled steel tube (CFST) columns subjected to full-range fire", *Engineering Structures*, 183: 265-280.

[14]. Thai Huu-Tai, Uy Brian, Khan Mahbub, Tao Zhong, Mashiri Fidelis (2014), "Numerical modelling of concrete-filled steel box columns incorporating high strength materials", *Journal of Constructional Steel Research*, 102: 256-265.

[15]. Wang Wen-Da, Han Lin-Hai, Zhao Xiao-Ling (2009), "Analytical behavior of frames with steel beams to concrete-filled steel tubular column", *Journal of Constructional Steel Research*, 65 (3): 497-508.

[16]. Thai Huu-Tai, Kim Seung-Eock (2011), "Second-order inelastic dynamic analysis of steel frames using fiber hinge method", *Journal of Constructional Steel Research*, 67 (10): 1485-1494.

[17]. Thai Huu-Tai, Kim Seung-Eock (2008), "Second-order inelastic dynamic analysis of three-dimensional cable-stayed bridges", *Steel Str*, 8: 205-214.

[18]. [Thai Huu-Tai, Kim Seung-Eock (2015), "Second-order distributed plasticity analysis of steel frames with semi-rigid connections", *Thin-Walled Structures*, 94: 120-128.

[19]. Chen Wai-Fah, Lui E. M. (1987), *Structural Stability: Theory and Implementation*, New York: Elsevier.

[20]. Kim Seung-Eock, Choi Se-Hyu (2001), "Practical advanced analysis for semi-rigid space frames", *International journal of solids and structures*, 38 (50-51): 9111-9131.

[21]. Thai Huu-Tai, Kim Seung-Eock (2011), "Nonlinear inelastic analysis of concrete-filled steel tubular frames", *Journal of Constructional Steel Research*, 67 (12): 1797-1805.

[22]. Mander John B, Priestley Michael JN, Park R (1988), "Theoretical stress-strain model for confined concrete", *Journal of structural engineering*, 114 (8): 1804-1826.

[23]. Liang Qing Quan (2009), "Performance-based analysis of concrete-filled steel tubular beam–columns, Part I: Theory and algorithms", *Journal of Constructional Steel Research*, 65 (2): 363-372.

[24]. Yang Yeong-Bin, Shieh Ming-Shan (1990), "Solution method for nonlinear problems with multiple critical points", *AIAA journal*, 28 (12): 2110-2116.

[25]. [Han Lin-Hai, Wang Wen-Da, Zhao Xiao-Ling (2008), "Behaviour of steel beam to concrete-filled SHS column frames: Finite element model and verifications", *Engineering Structures*, 30 (6): 1647-1658.